Materials and Structures (2018)51:15
https://doi.org/10.1617/s11527-018-1137-8

ORIGINAL ARTICLE

# Establishment and experimental validation of an updated predictive equation for the development and lap-spliced length of GFRP bars in concrete

**Mehrollah Rakhshanimehr · Seyed Roohollah Mousavi · M. Reza Esfahani · Saeed Farahi Shahri**

Received: 6 May 2017 / Accepted: 5 January 2018


**Abstract** Glass fibre-reinforced polymer (GFRP) reinforcement due to its physical and mechanical behavior has a completely different bond behavior compared to the steel bars. In this paper, an equation is proposed to predict the splice length in GFRP-reinforced concrete beams. First, equations for the local bond strength and displacement modulus of GFRP bars are obtained by using the eccentric and concentric pull-out test results given in the literature. Then, an equation is derived for the bond strength of spliced GFRP bars in beams. In the derivation of this equation, the non-uniform distribution of the bond stress along the splice length and the effect of elastic modulus of GFRP bars are taken into account. Compared to other available equations and design guidelines, the proposed equation for bond strength calculation shows good agreement with the experimental results. Using the proposed equation for bond strength, an equation is also proposed for the splice length of GFRP bars.

**Keywords** Bond strength · FRP bars · Modulus of displacement · Reinforced concrete beams · Splice length

**List of symbols**

| | |
|---|---|
| $A_b$ | Sectional area of longitudinal reinforcing bar |
| $A_t$ | Sectional area of one leg of transverse reinforcement |
| $C$ | Minimum of $C_x$, $C_y$, and $(C_s + d_b)/2$ |
| $C_{Med}$ | Median of $C_x$, $C_y$, and $(C_s + d_b)/2$ |
| $C_s$ | Spacing between spliced bars |
| $C_x$ | Side cover of reinforcing bars |
| $C_y$ | Bottom cover of reinforcing bars |
| $d_b$ | Longitudinal bar diameter |
| $E_{frp}$ | Elastic modulus of FRP bars |
| $E_s$ | Elastic modulus of steel bars |
| $f'_c$ | Compressive strength of concrete |
| $f_{cr}$ | Cracking strength of concrete |
| $f_f$ | Experimental bar stress of reinforcement |
| $f_{frpu}$ | Ultimate tensile strength of FRP bars |
| $f_R$ | Factor to include the effect of relative rib area of steel bars |
| $K$ | Displacement modulus of FRP bars |
| $k_1$ | Bar location factor |
| $k_2$ | Concrete density factor |

M. Rakhshanimehr (✉)
Civil Engineering Department, Alzahra University, Tehran, Iran
e-mail: m.rakhshanimehr@alzahra.ac.ir

S. R. Mousavi · S. Farahi Shahri
Civil Engineering Department, University of Sistan and Baluchestan, Zahedan, Iran
e-mail: s.r.mousavi@eng.usb.ac.ir

S. Farahi Shahri
e-mail: saeed_farahi@pgs.usb.ac.ir

M. R. Esfahani
Civil Engineering Department, Ferdowsi University of Mashhad, Mashhad, Iran
e-mail: esfahani@um.ac.ir

Published online: 17 January 2018

| | |
|---|---|
| $k_3$ | Bar size factor |
| $k_4$ | Bar fiber factor |
| $k_5$ | Bar surface profile factor |
| $K_{tr}$ | Transverse reinforcement index |
| $l_d$ | Splice length |
| $S$ | Spacing of transverse reinforcement |
| $S(x)$ | Slip between bar and concrete |
| $T$ | Maximum tensile force |
| $u_{ave}$ | Average bond stress |
| $u_c$ | Local bond strength |
| $u_m$ | The average bond stress at failure |
| $u_{max}$ | Maximum bond stress |
| $u_{min}$ | Minimum bond stress |
| $u_{(x)}$ | Bond stress over the splice length |
| $\alpha$ | Bar location factor |

## 1 Introduction

The physical and mechanical behavior of glass fibre-reinforced polymer (GFRP) reinforcement such as elastic behavior of GFRP bars (up to the point of failure), small elastic modulus, non-homogeneous properties and surface properties of these bars have caused them to have a completely different bond behavior compared to the steel bars. For instance, it is declared that steel bars have a better bond behavior in concrete than FRP bars [1, 2]. Accordingly, a change in the traditional design philosophy of concrete structures is needed for GFRP reinforcement [3].

Lin and Zhang [4] have given a review of some bond stress-slip models for FRP rebars in concrete, as well as some models for traditional steel rebars which might be appropriate for numerical analysis of concrete structures reinforced by FRP.

The lap-splice length of reinforcing bars is one of the practical aspects of the bond between concrete and reinforcing bars. The CAN/CSA S806-02 and CAN/CSA S6-06 code provisions and ACI 440.1R-06 guidelines determine the tensile splice length by multiplying the development length by either 1.6 [5, 6] or 1.3 [3], respectively. Darwin et al. [7] tried to formulate design criteria that incorporate a reliability–based strength reduction factor that allows the calculation of a single value for both splice and development length. On the other hand, many studies have shown that the bond strength in development lengths and splices may not be different [8].

FRP reinforcing bars are produced with different types of surface properties such as sand-coated, spiral wrapped, helical/ribbed and indented. The CAN/CSA S806-02 code specifies different factors for different bar surface properties for evaluating the bond strength of FRP bars [5]. Esfandeh et al. [9] demonstrated that increase in the surface roughness of the FRP rebars leads to a substantial effect on the bonding strength. However, Wambeke and Shield [10] and Mosley et al. [2] reported that the bar surface properties do not seem to affect the bond strength of FRP bars in concretes.

In this study, an approach similar to that proposed by Esfahani and Rangan [11] is used to extract a new analytical model for the calculation of bond strength between concrete and GFRP bars in lap-splices. Different parameters which affect the bond strength of spliced GFRP bars will be taken into account, e.g. bar diameter, the ratios between side cover, bottom cover, and spacing between the spliced bars, the modulus of elasticity of GFRP bars, and the non-uniform bond stress distribution along the spliced bars. Based on the proposed model for bond strength, a simple and practical equation is derived to predict the splice length of GFRP bars. The results of proposed equation are compared with available experimental results [2, 12–18].

## 2 Development of bond strength models of steel bars for GFRP bars

### 2.1 Equations for steel bond strength calculation

As shown in Fig. 1, dotted line indicates the average value of bond stress distribution, defined as equivalent uniform bond stress. Moreover, local bond strength is the maximum bond stress experienced by the rebar-concrete interface (see Fig. 1). Local bond strength and equivalent uniform bond stress are determined with eccentric pull-out and beam tests, respectively. Esfahani and Kianoush [19] proposed the following equation to calculate the equivalent uniform bond stress along the splice length of steel bars at failure:

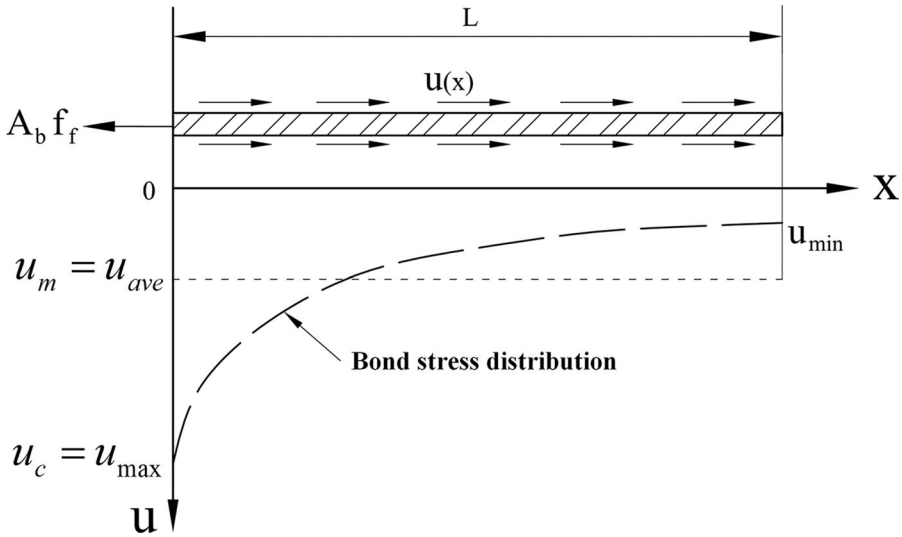


**Fig. 1** Bond stress distribution along spliced bars

$$u_m = u_c \frac{1 + 1/M}{1.85 + 0.024\sqrt{M}} \left(0.88 + 0.12 \frac{C_{\text{Med}}}{C}\right) \left(1 + 0.015\, f_{\text{R}} \frac{A_{\text{t}} A_{\text{b}}}{\text{CS}}\right) \quad (1)$$

where, $u_c$ is the local bond strength in MPa given by:

$$u_c = 2.7 \frac{C/d_{\text{b}} + 0.5}{C/d_{\text{b}} + 3.6} \sqrt{f'_c} \quad (2)$$

Also

$$M = \text{Cosh}\left(0.0022 l_d \sqrt{3 \frac{f'_c}{d_{\text{b}}}}\right) \quad (3)$$

In Eq. (1), $C_{\text{Med}}$ is the median of $C_x$, $C_y$, and $(C_S + d_{\text{b}})/2$; $C$ is the minimum of $C_x$, $C_y$, and $(C_S + d_{\text{b}})/2$; $C_x$ is the side cover, $C_y$ is the bottom cover of reinforcing bars and $C_s$ is the spacing between spliced bars in mm. $l_d$ is the splice length in mm; $d_{\text{b}}$ is the bar diameter in mm; and $f'_{\text{c}}$ is the compressive strength of concrete in MPa. $A_{\text{b}}$ is the area of longitudinal reinforcing bar in mm$^2$; $A_{\text{t}}$ is the area of one leg of transverse reinforcement in mm$^2$; $S$ is the spacing of transverse reinforcement in mm; and $f_{\text{R}}$ is a factor to include the effect of relative rib area of steel bars on bond strength.

In Eq. (1), the expressions $(1 + 1/M)/(1.85 + 0.024\sqrt{M})$, $(0.88 + 0.12[C_{\text{Med}}/C])$ and $(1 + 0.015 f_{\text{R}} A_{\text{t}} A_{\text{b}}/CS)$ account for the bond stress distribution along the reinforcing bar, the influence of the ratios between side cover, bottom cover, and the spacing between the spliced bars, and the effect of transverse reinforcement along the splice length on bond strength, respectively.

## 2.2 Local bond between concrete and GFRP bars

The interaction between concrete and reinforcement consists of a shear and normal stress acting on the rebar-concrete interface. The normal component produces the cracking of the concrete cover. Tepfers [20] modeled the normal force component and its surrounding concrete as a partly cracked thick cylinder under internal pressure. In this theory, it was assumed that an un-cracked concrete ring confined the cracked concrete and the reinforcing bar and resisted the bursting stresses radiating outwards from the bar at an angle $\alpha$ to the bar axis.

Esfahani and Rangan [21] proposed Eq. (2) for local bond strength of steel bars. This equation is based on Tepfers [20] partly cracked thick cylinder theory and eccentric pullout test results. Similar to the analysis used by Esfahani and Rangan [21] and using the eccentric pullout test results of GFRP bars [22–24], the following equation is obtained for the local bond strength of GFRP bars:

$$u_c = 2.3 \frac{C/d_{\text{b}} + 0.5}{C/d_{\text{b}} + 1.4} \sqrt{f'_{\text{c}}} \quad (4)$$

Table 1 compares Eq. (4) with the test results. The comparison shows that, Eq. (4) correlates well with the test results.

**Table 1** Comparison of local bond stress obtained from the proposed equation with the experimental data

| Reference | $C/d_b$ | $\left(u_c/\sqrt{f'_c}\right)_{test}$ | $\left(u_c/\sqrt{f'_c}\right)_{theo}$ | $(u_c)_{test}/(u_c)_{theo}$ |
|---|---|---|---|---|
| Tepfers and Karlsson [22] | 1.10 | 6.73 | 4.91 | 1.37 |
| | 1.10 | 4.36 | 4.91 | 0.89 |
| | 1.60 | 5.82 | 5.45 | 1.07 |
| | 1.60 | 4.73 | 5.45 | 0.87 |
| | 1.60 | 5.82 | 5.45 | 1.07 |
| | Mean | | | 1.05 |
| | SD | | | 0.20 |
| Tepfers et al. [23] | 2.20 | 6.36 | 5.75 | 1.11 |
| | 2.20 | 7.27 | 5.75 | 1.27 |
| | 1.70 | 6.00 | 5.45 | 1.10 |
| | 1.70 | 4.91 | 5.45 | 0.90 |
| | 1.70 | 5.82 | 5.45 | 1.07 |
| | 1.60 | 6.18 | 5.45 | 1.13 |
| | 1.60 | 5.64 | 5.45 | 1.03 |
| | 1.60 | 5.45 | 5.45 | 1.00 |
| | 1.60 | 5.27 | 5.45 | 0.97 |
| | 1.20 | 4.36 | 5.02 | 0.87 |
| | 1.20 | 4.91 | 5.02 | 0.98 |
| | Mean | | | 1.04 |
| | SD | | | 0.11 |
| Esfahani et al. [24] | 1.89 | 4.64 | 5.58 | 0.83 |
| | 1.89 | 4.85 | 5.58 | 0.87 |
| | 3.14 | 5.96 | 6.15 | 0.97 |
| | 3.14 | 6.04 | 6.15 | 0.98 |
| | Mean | | | 0.91 |
| | SD | | | 0.07 |
| All | Mean | | | 1.02 |
| | SD | | | 0.14 |

### 2.3 Bond stress distribution parameter of GFRP bars

As mentioned earlier, the expression of $(1 + 1/M)/(1.85 + 0.024\sqrt{M})$ in Eq. (1) accounts for the bond stress distribution along the reinforcing bar. Because the elastic modulus of GFRP bars is much lower than that of steel bars and also their surface properties are different, the bond stress distribution of GFRP bars differs from that of steel bars. Therefore, Eq. (3) used for steel bars, should be modified for GFRP bars. According to Esfahani and Rangan [11], the parameter $M$ was originally defined by the following equation:

$$M = \frac{u_{max}}{u_{min}} = \mathrm{Cosh}\left(jl_d/2\right) \quad (5)$$

where $j = (K\pi d_b/A_b E_s)^{1/2}$, $u_{max}$ and $u_{min}$ are the maximum and minimum bond stresses over the splice length in MPa, respectively, $A_b$ is the area of longitudinal reinforcing bar in mm$^2$, $E_s$ is the elastic modulus of steel bars in MPa, $l_d$ is the splice length in mm, $K$ is the displacement modulus in N/mm$^3$ and $d_b$ is the bar diameter in mm. Figure 1 illustrates the distribution of bond stress along a single splice as well as $u_{ave}$, $u_{max}$ and $u_{min}$ bond stresses.

Equation (5) is obtained by using the displacement modulus theory [11]. As shown in Fig. 2, the main concept of the displacement modulus theory is based on the linear relationship between bond stress and slip and also the actual displacement of reinforcement or the local deformation in the bond zone around the

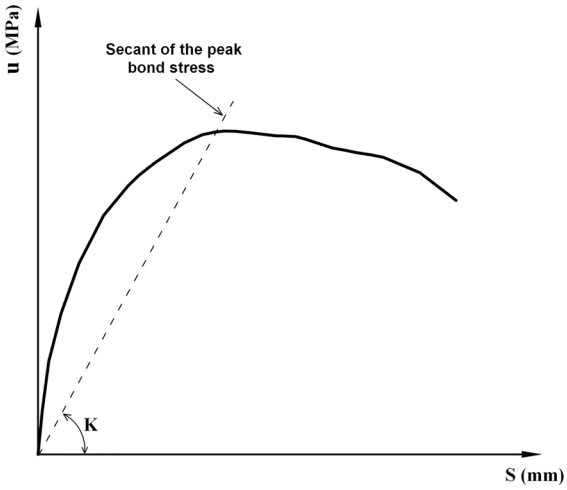


**Fig. 2** Determination of the displacement modulus $K$

reinforcement. Tepfers [20] applied this theory to determine the distribution of bond stress along lap-spliced steel bars in concrete. Aly [25] demonstrated that displacement modulus theory can also be used to determine the distribution of the bond stress for FRP bars. For these bars, parameter $j$ can be given by:

$$j_{\text{frp}} = \sqrt{\frac{K\pi d_{\text{b}}}{A_{\text{b}}E_{\text{frp}}}} \rightarrow j_{\text{frp}} = \sqrt{\frac{4K}{d_{\text{b}}E_{\text{frp}}}} \tag{6}$$

In Eq. (6), $K$ and $E_{\text{frp}}$ are the displacement modulus in N/mm$^3$ and the elastic modulus of FRP bars in MPa, respectively. The modulus of displacement $K$ can be determined from the bond stress-slip relationship. The secant modulus of bond stress versus slip relationship can represent the modulus of displacement [11, 12, 20, 25]. Substituting Eqs. (6) into (5) leads to the following equation for determining the value of $M$ for FRP bars:

$$M = \text{Cosh}\left(l_d\sqrt{\frac{K}{d_{\text{b}}E_{\text{frp}}}}\right) = \text{Cosh}\left(l_d\sqrt{\frac{K}{d_{\text{b}}E_{\text{s}}}\frac{E_{\text{s}}}{E_{\text{frp}}}}\right) \tag{7}$$

Similar to Esfahani and Rangan [11], by substituting $E_{\text{s}} = 210 \times 10^3$ MPa, in $K/d_{\text{b}}E_{\text{s}}$ of Eq. (7), the following equation is obtained:

$$M = \text{Cosh}\left(0.0022\, l_d\sqrt{\frac{E_s}{E_{\text{frp}}}}\sqrt{\frac{K}{d_{\text{b}}}}\right) \tag{8}$$

### 2.4 Determination of the displacement modulus ($K$) for GFRP bars

To account for the distribution of bond stresses over the development length or splice length, a theory based on a linear relationship between bond stress and slip has been used by researchers. The theory is known as Displacement Theory. The bond stress $u(x)$ over the splice length changes with the slip $S(x)$ between bar and concrete, i.e.:

$$u(x) = K \cdot S(x) \tag{9}$$

According to Losberg [26], the modulus of displacement, $K$, is the secant modulus of the relationship between bond stress and slip in a pullout test with short length of bar (Fig. 2). Using the test results, Tepfers [20] has shown that $K$ is proportional to the compressive strength of the concrete, i.e., $K = r\, f'_{\text{c}}$, where $r$ depends on the type of steel reinforcing bar.

The bond failure mechanism of GFRP bars is quite different from that of steel bars and the pullout failure mode of GFRP bars is usually different from that of steel bars. Davalos et al. [27] demonstrated that for relatively low concrete compressive strengths below 20 MPa, the bond strength is primarily determined based on the interface concrete failure which in turn is caused by induced cracking and tensile stresses such as occurred in steel bars. For concrete strengths greater than about 30 MPa, increasing of concrete strength leads to this fact that the interface mode of failure is caused by a combined effect of concrete and surface FRP material degradation, in which the FRP bar surface damage mainly plays the role of increasingly dominant factor in the failure. Hao et al. [28], Lee et al. [29] and Banea et al. [30] have shown that for concrete with compressive strength greater than 30 MPa, the shear strength between the fibers and the bar resin affects the bond strength and this shear strength is a function of the bar diameter. Aly [12] showed that in specimens with a compressive strength of 40 MPa, the value of $K$ decreases linearly with the increase of bar diameter.

In order to determine the value of displacement modulus $K$ in GFRP bars, the bond stress-slip relationship of concentric pullout tests from different studies [12, 29–31] are used and the secant at the peak bond stress of each curve is calculated (Fig. 2). It should be noted that bond length of rebar in pull-out test has a substantial effect on the displacement

modulus, so in order to have an almost uniform bond stress, the bond length is limited to 5 db in pull-out tests [21, 24]. The compressive strength of the concrete for these tests generally ranged from 25 to 65 MPa. For the test results, the values of $K$ are plotted against $d_b$ in Fig. 3. The best fit for the test results plotted in Fig. 3 is given by:

$$K = \frac{163.7}{(d_b)^{0.58}} \tag{10}$$

For brevity, the power of $d_b$ in Eq. (10) can be rounded to 0.5, thus Eq. (10) is replaced by the following equation:

$$K = \frac{135}{\sqrt{d_b}} \tag{11}$$

Figure 3 shows that Eq. (10) resembles Eq. (11). The mean of the test-predicted ratio of bar stresses using Eq. (11) is 1.00, with a coefficient of variation of 0.10. Equation (11) is used in Eq. (8) to account for the effect of bond stress distribution along the GFRP bars in bond strength calculation.

## 3 Bond strength of spliced GFRP bars

Equation (4) is based on the results of eccentric pull-out tests of short reinforcing bars (bond length between $3d_b$ and $6d_b$) embedded in concrete blocks conducted by Tepfers and Karlsson [22], Tepfers et al. [23] and Esfahani et al. [24]. The bonding action in

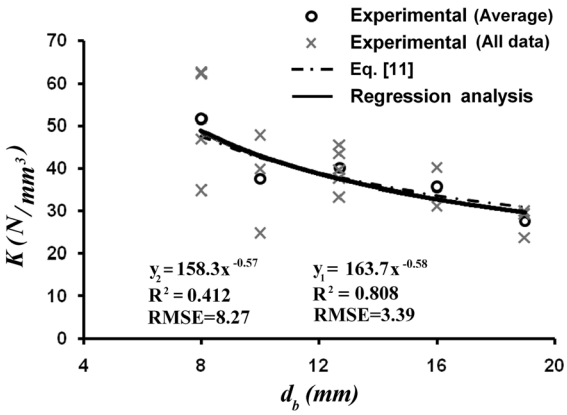


**Fig. 3** $K$ versus $d_b$ relationship (Note: Function $y_1$ is obtained by regression analysis on the mean of test data for each bar diameter. Function $y_2$ is obtained by regression analysis on all test data)

pull-out tests and short length splices in beams may not be the same. Esfahani and Rangan [11] discussed the differences between the bond strength of short length splices and the pull-out specimens. Furthermore, in short length splices, the distribution of the bond stresses over the bond length is almost uniform. For the practical length of spliced bars (between $40d_b$ and $60d_b$), the bond stresses are not uniform along the splice length. Esfahani and Rangan [11] used the parameter $M$ to account for the distribution of bond stresses over the splice length. Also, by examining different failure surfaces, Esfahani and Rangan [11] showed that the distribution of the bond stress along the splice length is influenced by the value of $C_{Med}/C$.

The bond strength equation of spliced bars without transverse reinforcement can be obtained by spliced beam test results carried out by Aly [12], Mosley et al. [2] and Harajli and Abouniaj [13], and the approach similar to that used by Esfahani and Rangan [11]. Details of the test results are summarized in Table 2. With respect to that bond failure of spliced bars is commonly caused by the splitting of the surrounding concrete [12, 32, 33], only the specimens with splitting mode of failure are utilized to predict the bond strength of lap-spliced GFRP bars. Darwin et al. [7] have ignored the results of spliced beam specimens with $l_d/d_b \leq 16$. Furthermore, According to Ghuayyum [34] findings, the maximum average bond strength for the GFRP bars increases with increasing the embedment length up to $40d_b$, but it is approximately constant for lengths greater than $60d_b$ ($l_d/d_b > 60$). So, the specimens with $l_d/d_b \leq 16$ and $l_d/d_b > 60$ are not considered in this study. The removal of these specimens do not hurt the overall evaluation, since specimens with such $l_d/d_b$ lower than 16 and higher than 60 are not used in practice.

Using the Esfahani and Rangan's approach [11], an equation for the bond strength of spliced bars in beams without transverse reinforcement is obtained as follows:

$$u_m = \frac{0.24}{\alpha} u_c \left(1 + \frac{1}{M}\right)\left(0.85 + 0.15\frac{C_{Med}}{C}\right) \tag{12}$$

where $\alpha$ is the bar location factor, which is 1.3 if there is more than 300 mm of concrete cast below the bar, otherwise $\alpha$ equals one [5, 19]. Parameters $M$, $u_c$ and $C_{Med}/C$ were defined earlier. More details for obtaining the bond strength equation can be seen elsewhere

**Table 2** Details of test specimens without transverse reinforcement

| Reference | Beam no. | Surface properties | $d_b$ (mm) | $C$ (mm) | $C_{Med}$ (mm) | $f'_c$ (MPa) | $u_{test}$ (MPa) | $l_d$ (mm) | $E_s/E_f$ |
|---|---|---|---|---|---|---|---|---|---|
| Mosley et al. [2] | B-G1-1 | W-SC | 16.0 | 20.5 | 38 | 38.6 | 2.29 | 457 | 4.90 |
| | B-G1-2 | W-SC | 16.0 | 20.5 | 38 | 29.0 | 1.73 | 305 | 4.90 |
| | B-G1-3 | W-SC | 16.0 | 38.0 | 60 | 41.2 | 2.95 | 305 | 4.90 |
| | B-G2-1 | R | 16.0 | 20.5 | 38 | 37.8 | 1.94 | 457 | 5.30 |
| | B-G2-2 | R | 16.0 | 20.5 | 38 | 27.0 | 1.77 | 305 | 5.30 |
| | B-G2-3 | R | 16.0 | 38.0 | 60 | 40.9 | 2.79 | 305 | 5.30 |
| | B-A-1 | R | 16.0 | 20.5 | 38 | 39.2 | 2.42 | 457 | 4.20 |
| | B-A-2 | R | 16.0 | 20.5 | 38 | 28.7 | 1.86 | 305 | 4.20 |
| | B-A-3 | R | 16.0 | 38.0 | 60 | 39.6 | 3.10 | 305 | 4.20 |
| Aly [12] | 6G70z-A22 | SC | 19.1 | 40.0 | 45 | 45.0 | 2.40 | 700 | 4.45 |
| | 6G70Z-A23 | SC | 19.1 | 40.0 | 45 | 43.0 | 2.54 | 700 | 4.45 |
| | 6G110Z-A24 | SC | 19.1 | 40.0 | 45 | 43.0 | 1.71 | 1100 | 4.45 |
| Harajli and Abouniaj [13] | R1.25L15 | G | 12.0 | 15.0 | 15 | 48.0 | 3.53 | 180 | 5.68 |
| | R1.25L20 | G | 12.0 | 15.0 | 15 | 48.0 | 3.19 | 240 | 5.68 |
| | R2L15 | G | 12.0 | 25.0 | 25 | 48.0 | 3.60 | 180 | 5.68 |
| | R2L20 | G | 12.0 | 25.0 | 25 | 48.0 | 3.67 | 240 | 5.68 |
| | R1.25L30 | G | 12.0 | 15.0 | 15 | 52.0 | 2.24 | 360 | 5.68 |

*G* grooved, *R* ribbed, *SC* sand coated, *W-SC* wrapped-sand coated

[11]. The average value of the test over predicted bond strength ratios using Eq. (12) is 0.96 with a standard deviation of 0.16 (Column 3 of Table 3).

According to ACI 440.1R-06 guidelines [3], the bond strength of GFRP reinforcing bars is calculated as follows:

$$\frac{u}{0.083\sqrt{f'_c}} = \frac{1}{\alpha}\left(4.0 + 0.3\frac{C}{d_b} + 100\frac{d_b}{l_d}\right) \quad (13)$$

where $\alpha = 1$ for bottom cast bars.

CAN/CSA S806-02 code [5] proposes the following equation for the development length of GFRP bars:

$$l_d = 1.15\frac{k_1k_2k_3k_4k_5}{d_{cs}}\frac{f_f}{\sqrt{f'_c}}A_b \quad (14)$$

Based on Eq. (14) and the equation $u = f_f A_b/(\pi d_b l_d)$, the bond strength of GFRP bars can be calculated as follows:

$$u = \frac{d_{cs}\sqrt{f'_c}}{1.15(k_1k_2k_3k_4k_5)\pi d_b} \quad (15)$$

Similarly, the bond strength of GFRP bars based on CAN/CSA S6-06 code [6] can be given by:

$$u = \frac{f_{cr}\left(d_{cs} + K_{tr}\frac{E_{frp}}{E_s}\right)}{0.45\pi d_b k_1 k_4} \quad (16)$$

All parameters in Eqs. (13)–(16) are defined in ACI 440.1R-06 guidelines [3], CAN/CSA S806-02 [5] and CAN/CSA S6-06 [6] codes. These parameters are also defined at the end of the paper. Using Eqs. (13)–(16), the predicted bond strengths of GFRP bars are calculated and compared with the test results. The average and standard deviation values of the test over predicted bond strength ratios for ACI 440.1R-06 guidelines [3], CAN/CSA S806-02 [5] and CAN/CSA S6-06 [6] codes are (0.67, 0.13), (0.68, 0.17) and (0.61, 0.18), respectively (Table 3). It can be concluded that, ACI 440.1R-06 guidelines [3], CAN/CSA S806-02 [5] and CAN/CSA S6-06 [6] codes overestimate the bond strength of GFRP bars in this series of test specimens.

**Table 3** Comparison of Eq. (12) and design equations with the test results (specimen without transverse reinforcement)

| Reference | Beam no. | $\frac{u_{test}}{u_{Eq.(12)}}$ | $\frac{u_{test}}{u_{ACI\,440.1R-06}}$ | $\frac{u_{test}}{u_{CSA\,S6-06}}$ | $\frac{u_{test}}{u_{CSA\,S806-02}}$ | $a_1$ $a_2$ |
|---|---|---|---|---|---|---|
| Mosley et al. [2] | B-G1-3 | 1.16 | 0.82 | 0.61 | 0.73 | 0.30 |
| | B-G2-3 | 1.12 | 0.78 | 0.58 | 0.69 | 0.29 |
| | B-A-3 | 1.21 | 0.88 | 0.82 | 0.78 | 0.31 |
| | B-A-1 | 1.11 | 0.89 | 0.95 | 0.89 | 0.30 |
| | B-A-2 | 0.86 | 0.65 | 0.85 | 0.80 | 0.33 |
| | B-G1-1 | 1.08 | 0.85 | 0.72 | 0.81 | 0.29 |
| | B-G2-1 | 0.93 | 0.73 | 0.62 | 0.69 | 0.29 |
| | B-G1-2 | 0.82 | 0.60 | 0.63 | 0.71 | 0.32 |
| | B-G2-2 | 0.89 | 0.64 | 0.67 | 0.79 | 0.32 |
| | Mean | 1.02 | 0.76 | 0.72 | 0.77 | 0.31 |
| | SD | 0.14 | 0.11 | 0.13 | 0.07 | 0.02 |
| Aly [12] | 6G70z-A22 | 0.83 | 0.57 | 0.37 | 0.41 | 0.25 |
| | 6G70Z-A23 | 0.90 | 0.62 | 0.40 | 0.45 | 0.25 |
| | 6G110Z-A24 | 0.62 | 0.48 | 0.27 | 0.30 | 0.25 |
| | Mean | 0.78 | 0.56 | 0.34 | 0.39 | 0.25 |
| | SD | 0.14 | 0.07 | 0.07 | 0.08 | 0.00 |
| Harajli and Abouniaj [13] | R1.25L15 | 1.03 | 0.55 | 0.75 | 0.88 | 0.32 |
| | R1.25L20 | 1.04 | 0.58 | 0.68 | 0.80 | 0.29 |
| | R2L15 | 0.93 | 0.55 | 0.53 | 0.63 | 0.32 |
| | R2L20 | 1.07 | 0.65 | 0.54 | 0.64 | 0.29 |
| | R1.25L30 | 0.79 | 0.48 | 0.46 | 0.54 | 0.25 |
| | Mean | 0.97 | 0.56 | 0.59 | 0.70 | 0.29 |
| | SD | 0.11 | 0.06 | 0.12 | 0.14 | 0.03 |
| All | Mean | 0.96 | 0.67 | 0.61 | 0.68 | 0.29 |
| | SD | 0.16 | 0.13 | 0.18 | 0.17 | 0.03 |

## 4 Comparison between experimental and calculated bond strengths

### 4.1 Specimens without transverse reinforcement

In this part of the study, new test results of specimens without transverse reinforcement [14, 15] as the validation data are compared with the proposed equation. Details of these test series are summarized in Table 4. Comparison between the bond strength values obtained from Eq. (12) with experimental results is presented in Table 5. The average and standard deviation values of the test over predicted bond strength ratios are 1.05 and 0.22, respectively.

The average and standard deviation values of the test over predicted bond strength ratios for ACI 440.1R-06 guidelines [3], CAN/CSA S806-02 [5] and CAN/CSA S6-06 [6] codes are (0.72, 0.14), (0.73, 0.26) and (0.62, 0.19), respectively (Table 5). It is observed that the predicted bond strength of GFRP bars is considerably larger than the experimental values, and the ACI 440.1R-06 [3], CAN/CSA S806-02 [5] and CAN/CSA S6-06 [6] overestimate the bond strength for this series of test specimens.

### 4.2 Specimens with transverse reinforcement

The bond strength of spliced GFRP bars confined with transverse reinforcement in different test series [12, 13, 16–18] has been calculated with Eq. (12). The details of the test specimens are given in Table 6. $u_{test}/u_{eq\ (12)}$ ratios are given in Column 3 of Table 7. The average and the standard deviation values of the experimental to calculated bond strength ratios for the specimens with transverse reinforcement are 1.25 and 0.29, respectively. It is seen that the experimental average bond strength of splices with transverse reinforcement is approximately 1.25 times the values

**Table 4** Details of recent test results presented by Choi et al. [14] and Pay et al. [15] (spliced bars without transverse reinforcement)

| Reference | Beam no. | Surface properties | $d_b$ (mm) | $C$ (mm) | $C_{Med}$ (mm) | $f'_c$ (MPa) | $u_{test}$ (MPa) | $l_d$ (mm) | $E_s/E_f$ |
|---|---|---|---|---|---|---|---|---|---|
| Choi et al. [14] | B-2As-L20db-c25 | SW | 12.7 | 25.4 | 30 | 30 | 4.17 | 254 | 4.9 |
| | B-2As-L30db-c25 | SW | 12.7 | 25.4 | 30 | 30 | 3.44 | 381 | 4.9 |
| | B-2As-L40db-c25 | SW | 12.7 | 25.4 | 30 | 30 | 3.15 | 508 | 4.9 |
| | B-2As-L55db-c25 | SW | 12.7 | 25.4 | 30 | 30 | 2.39 | 698.5 | 4.9 |
| | B-2Iso-L30db-c25 | SC | 12.7 | 25.4 | 30 | 30 | 3.3 | 381 | 4.76 |
| | B-2Iso-L40db-c25 | SC | 12.7 | 25.4 | 30 | 30 | 2.75 | 508 | 4.76 |
| | B-2Iso-L50db-c25 | SC | 12.7 | 25.4 | 30 | 30 | 2.15 | 635 | 4.76 |
| | B-2Iso-L60db-c25 | SC | 12.7 | 25.4 | 30 | 30 | 1.97 | 762 | 4.76 |
| | B-3K2-L30db-c25 | SC | 12.7 | 25.4 | 30 | 23 | 2.53 | 381 | 5.38 |
| | B-3K2-L45db-c25 | SC | 12.7 | 25.4 | 30 | 23 | 1.94 | 571.5 | 5.38 |
| | B-3K2-L60db-c25 | SC | 12.7 | 25.4 | 30 | 23 | 1.65 | 762 | 5.38 |
| | B-3K2-L30db-c13 | SC | 12.7 | 12.7 | 30 | 23 | 1.97 | 381 | 5.38 |
| | B-3K2-L30db-c51 | SC | 12.7 | 30 | 47.35 | 23 | 2.74 | 381 | 5.38 |
| | B-4K2-L30db-c25 | SC | 12.7 | 25.4 | 29.45 | 23 | 2.57 | 381 | 5.38 |
| | B-5K2-L30db-c25 | SC | 12.7 | 20.55 | 25.4 | 23 | 2.61 | 381 | 5.38 |
| | B-4K2-L45db-c25 | SC | 12.7 | 25.4 | 29.45 | 23 | 1.74 | 571.5 | 5.38 |
| | B-5K2-L45db-c25 | SC | 12.7 | 20.55 | 25.4 | 23 | 1.47 | 571.5 | 5.38 |
| | B-3As-L30db-c25 | SW | 12.7 | 25.4 | 30 | 23 | 3.09 | 381 | 4.9 |
| | B-3As-L45db-c25 | SW | 12.7 | 25.4 | 30 | 23 | 1.82 | 571.5 | 4.9 |
| | B-3As-L60db-c25 | SW | 12.7 | 25.4 | 30 | 23 | 2.09 | 762 | 4.9 |
| Pay et al. [15] | B-PG-8-18 | SC | 25.4 | 25.4 | 38 | 36.3 | 2.668 | 457 | 4.92 |
| | B-HG-8-18 | W-SC | 25.4 | 25.4 | 38 | 36.3 | 2.265 | 457 | 5.34 |
| | B-HG1-5-18 | W-SC | 15.88 | 20.6 | 38 | 36.3 | 2.440 | 457 | 4.76 |
| | B-HGO-5-18 | W-SC | 15.88 | 20.6 | 38 | 36.3 | 1.971 | 457 | 5.25 |
| | B-PG-5-18 | SC | 15.88 | 20.6 | 38 | 36.3 | 2.831 | 457 | 4.76 |
| | B-PG-8-36 | SC | 25.4 | 25.4 | 38 | 37.7 | 1.383 | 914 | 4.92 |
| | B-HG-8-36 | W-SC | 25.4 | 25.4 | 38 | 37.7 | 1.459 | 914 | 5.34 |
| | B-HG1-5-36 | W-SC | 15.88 | 20.6 | 38 | 37.7 | 1.324 | 914 | 4.76 |
| | B-HGO-5-36 | W-SC | 15.88 | 20.6 | 38 | 37.7 | 1.424 | 914 | 5.25 |
| | B-PG-5-36 | SC | 15.88 | 20.6 | 38 | 37.7 | 1.494 | 914 | 4.76 |
| | B-HG1-5-24 | W-SC | 15.88 | 20.6 | 38 | 32 | 1.750 | 610 | 4.76 |
| | B-HG2-5-24 | FT | 15.88 | 20.6 | 38 | 32 | 2.134 | 610 | 4.17 |
| | B-PG-5-24 | SC | 15.88 | 20.6 | 38 | 32 | 2.154 | 610 | 4.76 |
| | B-HG1-5-24b | W-SC | 15.88 | 20.6 | 38 | 32 | 1.893 | 610 | 4.76 |
| | B-PG-5-24b | SC | 15.88 | 20.6 | 38 | 32 | 2.277 | 610 | 4.76 |
| | B-HG1-5-12 | W-SC | 15.88 | 20.6 | 38 | 28.8 | 2.459 | 305 | 4.76 |
| | B-PG-5-12 | SC | 15.88 | 20.6 | 38 | 28.8 | 2.733 | 305 | 4.76 |
| | B-HG-8-24 | W-SC | 25.4 | 25.4 | 38 | 28.8 | 1.728 | 610 | 5.34 |
| | B-HG-8-54 | W-SC | 25.4 | 25.4 | 38 | 28.8 | 1.055 | 1372 | 5.34 |
| | B-HG1-5-12b | W-SC | 15.88 | 20.6 | 38 | 28.8 | 3.123 | 305 | 4.76 |
| | B-PG-5-12b | SC | 15.88 | 20.6 | 38 | 28.8 | 3.500 | 305 | 4.76 |
| | B-HG-8-24b | W-SC | 25.4 | 25.4 | 38 | 28.8 | 1.915 | 610 | 5.34 |

*FT* fabric texture, *SC* sand coated, *SW* spiral wrapped, *W-SC* wrapped-sand coated

**Table 5** Analysis of recent test results presented by Choi et al. [14] and Pay et al. [15]

| Reference | Beam no. | $\frac{u_{test}}{u_{eq.(12)}}$ | $\frac{u_{test}}{u_{ACI440.1R-06}}$ | $\frac{u_{test}}{u_{CSA\,S6-06}}$ | $\frac{u_{test}}{u_{CSA\,S806-02}}$ | $a_1$ $a_2$ |
|---|---|---|---|---|---|---|
| Choi et al. [14] | B-2As-L20db-c25 | 1.48 | 0.94 | 0.78 | 0.88 | 0.30 |
| | B-2As-L30db-c25 | 1.39 | 0.94 | 0.65 | 0.73 | 0.27 |
| | B-2As-L40db-c25 | 1.34 | 0.96 | 0.59 | 0.66 | 0.25 |
| | B-2As-L55db-c25 | 1.04 | 0.80 | 0.45 | 0.50 | 0.25 |
| | B-2Iso-L30db-c25 | 1.33 | 0.90 | 0.62 | 0.70 | 0.27 |
| | B-2Iso-L40db-c25 | 1.17 | 0.83 | 0.52 | 0.58 | 0.25 |
| | B-2Iso-L50db-c25 | 0.93 | 0.70 | 0.40 | 0.45 | 0.25 |
| | B-2Iso-L60db-c25 | 0.86 | 0.68 | 0.37 | 0.42 | 0.25 |
| | B-3K2-L30db-c25 | 1.18 | 0.79 | 0.54 | 0.61 | 0.26 |
| | B-3K2-L45db-c25 | 0.96 | 0.70 | 0.42 | 0.47 | 0.25 |
| | B-3K2-L60db-c25 | 0.82 | 0.65 | 0.35 | 0.40 | 0.25 |
| | B-3K2-L30db-c13 | 0.92 | 0.64 | 0.70 | 0.79 | 0.31 |
| | B-3K2-L30db-c51 | 1.17 | 0.84 | 0.59 | 0.66 | 0.28 |
| | B-4K2-L30db-c25 | 1.21 | 0.80 | 0.55 | 0.62 | 0.26 |
| | B-5K2-L30db-c25 | 1.27 | 0.82 | 0.65 | 0.73 | 0.27 |
| | B-4K2-L45db-c25 | 0.86 | 0.63 | 0.37 | 0.42 | 0.25 |
| | B-5K2-L45db-c25 | 0.75 | 0.54 | 0.37 | 0.41 | 0.25 |
| | B-3As-L30db-c25 | 1.43 | 0.96 | 0.66 | 0.74 | 0.27 |
| | B-3As-L45db-c25 | 0.90 | 0.66 | 0.39 | 0.44 | 0.25 |
| | B-3As-L60db-c25 | 1.04 | 0.82 | 0.45 | 0.50 | 0.25 |
| | Mean | 1.10 | 0.78 | 0.52 | 0.59 | 0.26 |
| | SD | 0.22 | 0.13 | 0.13 | 0.15 | 0.02 |
| Pay et al. [15] | B-PG-8-18 | 1.29 | 0.69 | 1.11 | 1.56 | 0.31 |
| | B-HG-8-18 | 1.12 | 0.59 | 0.94 | 1.32 | 0.30 |
| | B-HG1-5-18 | 1.18 | 0.79 | 0.78 | 0.88 | 0.29 |
| | B-HGO-5-18 | 0.96 | 0.64 | 0.63 | 0.71 | 0.29 |
| | B-PG-5-18 | 1.36 | 0.92 | 0.91 | 1.02 | 0.29 |
| | B-PG-8-36 | 0.77 | 0.49 | 0.56 | 0.79 | 0.26 |
| | B-HG-8-36 | 0.82 | 0.51 | 0.60 | 0.84 | 0.26 |
| | B-HG1-5-36 | 0.67 | 0.54 | 0.42 | 0.47 | 0.27 |
| | B-HGO-5-36 | 0.73 | 0.58 | 0.45 | 0.50 | 0.27 |
| | B-PG-5-36 | 0.76 | 0.61 | 0.47 | 0.53 | 0.27 |
| | B-HG1-5-24 | 0.94 | 0.68 | 0.60 | 0.67 | 0.28 |
| | B-HG2-5-24 | 1.14 | 0.83 | 0.73 | 0.82 | 0.28 |
| | B-PG-5-24 | 1.16 | 0.83 | 0.73 | 0.83 | 0.28 |
| | B-HG1-5-24b | 0.79 | 0.56 | 0.50 | 0.56 | 0.28 |
| | B-PG-5-24b | 0.95 | 0.68 | 0.60 | 0.67 | 0.28 |
| | B-HG1-5-12 | 1.17 | 0.74 | 0.88 | 0.99 | 0.33 |
| | B-PG-5-12 | 1.30 | 0.82 | 0.98 | 1.10 | 0.33 |
| | B-HG-8-24 | 1.04 | 0.59 | 0.81 | 1.13 | 0.28 |
| | B-HG-8-54 | 0.69 | 0.49 | 0.49 | 0.69 | 0.26 |
| | B-HG1-5-12b | 1.14 | 0.72 | 0.86 | 0.97 | 0.33 |
| | B-PG-5-12b | 1.28 | 0.81 | 0.97 | 1.09 | 0.33 |
| | B-HG-8-24b | 0.89 | 0.50 | 0.69 | 0.97 | 0.28 |

**Table 5** continued

| Reference | Beam no. | $\frac{u_{test}}{u_{eq.(12)}}$ | $\frac{u_{test}}{u_{ACI\,440.1R-06}}$ | $\frac{u_{test}}{u_{CSA\,S6-06}}$ | $\frac{u_{test}}{u_{CSA\,S806-02}}$ | $a_1\,a_2$ |
|---|---|---|---|---|---|---|
| | Mean | 1.01 | 0.66 | 0.71 | 0.87 | 0.29 |
| | SD | 0.22 | 0.13 | 0.20 | 0.27 | 0.02 |
| All | Mean | 1.05 | 0.72 | 0.62 | 0.73 | 0.28 |
| | SD | 0.22 | 0.14 | 0.19 | 0.26 | 0.02 |

calculated by Eq. (12) given for splices without transverse reinforcement in Table 3. According to ACI 440.1R-06 [3], Darwin et al. [7] discussed about how confining steel bars with a high relative rib area can suitably raise the bond force in comparison with the same-size steel bars having a moderate relative rib area. Relative rib area of GFRP bars is very low, so it may leads to stop the enlargement of average bond strength due to presence of transverse reinforcement. This approach is supported by several investigations in this field [5, 10].

Table 7 also presents a comparison between bond strength values obtained from Eq. (12) and other available equations with experimental results for specimens with transverse reinforcement along the splice length. The average and standard deviation values of the experimental to calculated bond strength obtained by ACI 440.1R-06 guidelines [3], CAN/CSA S806-02 [5] and CAN/CSA S6-06 [6] codes are equal to (0.87, 0.20), (0.89, 0.42) and (0.72, 0.30), respectively. It can be concluded that, ACI 440.1R-06 guidelines [3], CAN/CSA S806-02 [5] and CAN/CSA S6-06 [6] codes overestimate the bond strength of this series of test specimens. According to Tables 5 and 7, it is observed that Eq. (12) calculates the bond strength more accurately than other equations. It may be due to the low relative rib area of GFRP bars used for the most of the specimens, such as sand coated specimens in [12] and helical wrapped specimens in [17]. It can be seen that for specimens with high relative rib area, the Eq. (12) presents a more conservative estimation of the bond strength rather than the other equations (such as ribbed specimens tested by Esfahani et al. [18]).

## 5 A proposed equation for determining the splice length

It was shown earlier that although Eq. (12) was initially developed for specimens without transverse reinforcement, it also gives reasonable and conservative results for specimens with transverse reinforcement. In addition, though the GFRP bars had different surface properties, the bond strengths calculated by the proposed equation for GFRP bars with different surface properties correlated well with the experimental results. The bar surface properties in different specimens are presented in Column 3 of Tables 2, 4 and 6.

Mosley et al. [2] have shown that bond strength is related to the modulus of elasticity of the reinforcement. One of the important advantages of the proposed equation in comparison with the ACI 440.1R-06 guidelines [3] is accounting for the elastic modulus in the bond strength calculations. Furthermore, in the proposed equation, a non-uniform bond stress distribution is assumed along the splice length.

In order to present an equation for splice length calculation, Eq. (12) is written as a function of the maximum tensile force of the reinforcement as follows:

$$\frac{T}{\pi d_b l_d} = \frac{0.24}{\alpha} u_c \left(1 + \frac{1}{M}\right)\left(0.85 + 0.15\frac{C_{Med}}{C}\right) \quad (17)$$

Equation (17) can be given by:

$$\frac{T}{\pi d_b l_d} = \frac{u_c}{\alpha} a_1 a_2 \quad (18)$$

where,

$$a_1 = 0.24\left(1 + \frac{1}{M}\right) \quad (19)$$

**Table 6** Details of spliced bars with transverse reinforcement

| Reference. | Beam no. | Surface properties | $d_b$ (mm) | $C$ (mm) | $C_{Med}$ (mm) | $f'_c$ (MPa) | $u_{test}$ (MPa) | $l_d$ (mm) | $E_s/E_f$ | $A_t$ (mm) | $S$ (mm) |
|---|---|---|---|---|---|---|---|---|---|---|---|
| Aly [12] | 6G50N-A8 | SC | 19.1 | 40 | 45 | 41 | 3.60 | 500 | 4.45 | 50.27 | 150 |
| | 6G70N-A9 | SC | 19.1 | 40 | 45 | 43 | 3.28 | 700 | 4.45 | 50.27 | 150 |
| | 6G80N-A10 | SC | 19.1 | 40 | 45 | 41 | 3.30 | 800 | 4.45 | 50.27 | 150 |
| | 6G70L-A25 | SC | 19.1 | 40 | 45 | 43 | 2.95 | 700 | 4.45 | 50.27 | 300 |
| | 6G70N-A26 | SC | 19.1 | 40 | 45 | 43 | 3.28 | 700 | 4.45 | 50.27 | 150 |
| | 6G70N-KW28 | SC | 19.1 | 25 | 40 | 45 | 2.83 | 700 | 4.45 | 50.27 | 150 |
| | 6G70N-FX29 | SC | 19.1 | 25 | 45 | 43 | 3.18 | 700 | 4.45 | 50.27 | 150 |
| | 6G70N-KX30 | SC | 19.1 | 40 | 45 | 43 | 3.28 | 700 | 4.45 | 50.27 | 150 |
| | 6G70N-PX31 | SC | 19.1 | 45 | 51.35 | 45 | 2.91 | 700 | 4.45 | 50.27 | 150 |
| | 6G70N-KY32 | SC | 19.1 | 40 | 51.35 | 43 | 3.60 | 700 | 4.45 | 50.27 | 150 |
| | 6G70N-PY33 | SC | 19.1 | 51.35 | 70 | 45 | 3.21 | 700 | 4.45 | 50.27 | 150 |
| Harajli and Abouniaj [13] | R1.25L20-C | G | 12.0 | 15.0 | 15 | 52.0 | 4.18 | 240 | 5.68 | 50 | 60 |
| Mousavi [16] | B-1 | SC | 16.0 | 25.0 | 25 | 40.0 | 3.20 | 400 | 3.50 | 50 | 150 |
| | B-2 | SC | 16.0 | 30.0 | 30 | 40.0 | 3.02 | 279 | 5.10 | 50 | 50 |
| | B-3 | SC | 12.0 | 13.5 | 25 | 70.0 | 4.19 | 400 | 3.50 | 50 | 150 |
| | B-4 | SC | 12.0 | 13.5 | 25 | 70.0 | 5.14 | 400 | 3.50 | 50 | 100 |
| Tighiouart et al. [17] | A460-1 | HW | 12.7 | 30.0 | 30 | 42.0 | 3.73 | 460 | 4.67 | 100 | 80 |
| | A460-2 | HW | 12.7 | 30.0 | 30 | 42.0 | 3.83 | 460 | 4.67 | 100 | 80 |
| | A540-1 | HW | 12.7 | 30.0 | 30 | 42.0 | 2.52 | 540 | 4.67 | 100 | 80 |
| | A540-2 | HW | 12.7 | 30.0 | 30 | 42.0 | 3.35 | 540 | 4.67 | 100 | 80 |
| | B-675-1 | HW | 15.9 | 30.0 | 30 | 42.5 | 3.11 | 675 | 4.67 | 100 | 80 |
| | B-675-2 | HW | 15.9 | 30.0 | 30 | 42.5 | 3.14 | 675 | 4.67 | 100 | 80 |
| | B-870-1 | HW | 15.9 | 30.0 | 30 | 42.5 | 2.44 | 870 | 4.67 | 100 | 80 |
| | B-870-2 | HW | 15.9 | 30.0 | 30 | 42.5 | 2.64 | 870 | 4.67 | 100 | 80 |
| Esfahani et al. [18] | R16-40-S150 | R | 16 | 20.5 | 25 | 41 | 3.2 | 400 | 3.5 | 50 | 150 |
| | R16-40-S100 | R | 16 | 20.5 | 25 | 41 | 4.18 | 400 | 3.5 | 50 | 100 |
| | R16-40-S50 | R | 16 | 20.5 | 25 | 41 | 5.18 | 400 | 3.5 | 50 | 50 |
| | R12-40-S150 | R | 12 | 13.5 | 25 | 41 | 4.31 | 400 | 3.5 | 50 | 150 |
| | R12-40-S100 | R | 12 | 13.5 | 25 | 41 | 5.14 | 400 | 3.5 | 50 | 100 |
| | R12-40-S50 | R | 12 | 13.5 | 25 | 41 | 6.22 | 400 | 3.5 | 50 | 50 |
| | R12-70-S150 | R | 12 | 13.5 | 25 | 72 | 4.19 | 400 | 3.5 | 50 | 150 |
| | R12-70-S100 | R | 12 | 13.5 | 25 | 72 | 5.14 | 400 | 3.5 | 50 | 100 |
| | R12-70-S50 | R | 12 | 13.5 | 25 | 72 | 6.64 | 400 | 3.5 | 50 | 50 |

*G* grooved, *HW* helical wrapped, *R* ribbed, *SC* sand coated

$$a_2 = \left(0.85 + 0.15\frac{C_{\text{Med}}}{C}\right) \tag{20}$$

By replacing $u_c$ from Eqs. (4) into (18), the following equation is obtained:

$$T = \frac{7.22}{\alpha} d_b \frac{C/d_b + 0.5}{C/d_b + 1.4} l_d \sqrt{f'_c} a_1 a_2 \tag{21}$$

By assuming $a_3 = 7.22 d_b \frac{C/d_b + 0.5}{C/d_b + 1.4}$, the value of $l_d$ is obtained by:

**Table 7** Comparison of Eq. (12) and design equations with the test results (specimen with transverse reinforcement)

| Reference | Beam no. | $\frac{u_{test}}{u_{eq.(12)}}$ | $\frac{u_{test}}{u_{ACI\,440.1R-06}}$ | $\frac{u_{test}}{u_{CSA\,S6-06}}$ | $\frac{u_{test}}{u_{CSA\,S806-02}}$ | $a_1$ $a_2$ |
|---|---|---|---|---|---|---|
| Aly [12] | 6G50N-A8 | 1.22 | 0.79 | 0.57 | 0.65 | 0.27 |
| | 6G70N-A9 | 1.16 | 0.80 | 0.50 | 0.58 | 0.25 |
| | 6G80N-A10 | 1.21 | 0.87 | 0.52 | 0.60 | 0.25 |
| | 6G70L-A25 | 1.04 | 0.72 | 0.46 | 0.52 | 0.25 |
| | 6G70N-A26 | 1.16 | 0.80 | 0.50 | 0.58 | 0.25 |
| | 6G70N-KW28 | 1.02 | 0.70 | 0.58 | 0.67 | 0.27 |
| | 6G70N-FX29 | 1.14 | 0.80 | 0.67 | 0.77 | 0.28 |
| | 6G70N-KX30 | 1.16 | 0.80 | 0.50 | 0.58 | 0.25 |
| | 6G70N-PX31 | 0.98 | 0.69 | 0.44 | 0.50 | 0.25 |
| | 6G70N-KY32 | 1.24 | 0.88 | 0.55 | 0.63 | 0.26 |
| | 6G70N-PY33 | 1.02 | 0.75 | 0.48 | 0.55 | 0.26 |
| | Mean | 1.12 | 0.78 | 0.52 | 0.60 | 0.26 |
| | SD | 0.09 | 0.06 | 0.06 | 0.08 | 0.01 |
| Harajli and Abouniaj [13] | R1.25L20-C | 1.31 | 0.75 | 0.79 | 1.00 | 0.29 |
| Mousavi [16] | B-1 | 1.11 | 0.72 | 0.93 | 1.15 | 0.30 |
| | B-2 | 0.96 | 0.57 | 0.65 | 0.81 | 0.30 |
| | B-3 | 1.11 | 0.81 | 1.02 | 1.30 | 0.30 |
| | B-4 | 1.36 | 1.00 | 1.21 | 1.59 | 0.30 |
| | Mean | 1.14 | 0.78 | 0.95 | 1.21 | 0.30 |
| | SD | 0.17 | 0.18 | 0.23 | 0.32 | 0.00 |
| Tighiouart et al. [17] | A460-1 | 1.30 | 0.91 | 0.59 | 0.67 | 0.25 |
| | A460-2 | 1.34 | 0.94 | 0.61 | 0.68 | 0.25 |
| | A540-1 | 0.90 | 0.65 | 0.40 | 0.45 | 0.25 |
| | A540-2 | 1.20 | 0.87 | 0.53 | 0.60 | 0.25 |
| | B-675-1 | 1.16 | 0.82 | 0.49 | 0.58 | 0.25 |
| | B-675-2 | 1.17 | 0.82 | 0.50 | 0.58 | 0.25 |
| | B-870-1 | 0.92 | 0.69 | 0.38 | 0.45 | 0.24 |
| | B-870-2 | 1.00 | 0.75 | 0.42 | 0.49 | 0.24 |
| | Mean | 1.12 | 0.81 | 0.49 | 0.56 | 0.25 |
| | SD | 0.16 | 0.10 | 0.09 | 0.09 | 0.00 |
| Esfahani et al. [18] | R16-40-S150 | 1.11 | 0.71 | 0.75 | 0.89 | 0.29 |
| | R16-40-S100 | 1.45 | 0.92 | 0.96 | 1.16 | 0.29 |
| | R16-40-S50 | 1.80 | 1.14 | 1.11 | 1.44 | 0.29 |
| | R12-40-S150 | 1.53 | 1.08 | 1.13 | 1.36 | 0.30 |
| | R12-40-S100 | 1.83 | 1.29 | 1.30 | 1.62 | 0.30 |
| | R12-40-S50 | 2.21 | 1.56 | 1.42 | 1.97 | 0.30 |
| | R12-70-S150 | 1.12 | 0.79 | 0.83 | 1.00 | 0.30 |
| | R12-70-S100 | 1.38 | 0.97 | 0.98 | 1.23 | 0.30 |
| | R12-70-S50 | 1.78 | 1.26 | 1.15 | 1.58 | 0.30 |
| | Mean | 1.58 | 1.08 | 1.07 | 1.36 | 0.30 |
| | SD | 0.36 | 0.27 | 0.21 | 0.34 | 0.00 |
| All | Mean | 1.25 | 0.87 | 0.72 | 0.89 | 0.27 |
| | SD | 0.29 | 0.20 | 0.30 | 0.42 | 0.02 |

$$l_d = \frac{\alpha T}{\left(a_3\sqrt{f'_c}\right)a_1 a_2} \tag{22}$$

The value of $a_1a_2$ can be determined using experimental results [19]. The values of $a_1a_2$ for specimens with and without transverse reinforcement over the spliced length are given in Column 7 of Tables 3, 5 and 7. In Eq. (22), the parameter $a_2$ as given by Eq. (20) accounts for the effect of $C_{\text{Med}}/C$ on bond strength. Previous studies have shown that when adequate $C_{\text{Med}}/C$ is used, the bond stress becomes more uniform, and thus the bond strength increases [11, 12]. The parameter $a_1$ accounts for the effect of bond stress distribution over the splice length. As the splice length increases, the bond stress distribution becomes less uniform. Subsequently, the parameter $M$ increases and the value of $a_1$ decreases. On the other hand, $C_{\text{Med}}/C$ increases the uniformity of the bond stress distribution and the bond strength. Therefore, it is reasonable to keep the multiple of $a_1a_2$ constant from a design point of view. The average value of $a_1a_2$ for all test results presented in Tables 3, 5 and 7 can be given by:

$$a_1 a_2 = 0.28 \tag{23}$$

Substituting Eqs. (23) into (22) leads to:

$$l_d = \frac{\alpha T}{\left(\beta\sqrt{f'_c}\right)} \tag{24}$$

Parameter $\beta$ in Eq. (24) is obtained by the following equation:

$$\beta = 2\frac{C/d_{\text{b}} + 0.5}{C/d_{\text{b}} + 1.4}d_{\text{b}} \tag{25}$$

In Eq. (24), $T$ is the tensile force of GFRP bars and is given by:

$$T = A_b \times f_{\text{frpu}} \tag{26}$$

In this equation, $f_{\text{frpu}}$ is the ultimate tensile strength of GFRP bars in MPa and $A_{\text{b}}$ is the area of GFRP reinforcement in mm$^2$. By introducing Eqs. (26) into (24), the following equation is obtained:

$$l_d = \frac{\alpha A_b f_{\text{frpu}}}{\left(\beta\sqrt{f'_c}\right)} \tag{27}$$

Equation (27) can be used to determine the splice length of GFRP bars. This equation will only be valid if the product of $a_1a_2$ is equal to 0.28. In this case, by introducing the values of $a_1$ and $a_2$ obtained from Eqs. (19) and (20), the following equation can be written:

$$0.28 = 0.24\left(1 + \frac{1}{M}\right)\left(0.85 + 0.15\frac{C_{\text{Med}}}{C}\right) \tag{28}$$

Solving Eq. (28) for $C_{\text{Med}}/C$ leads to:

$$\frac{C_{\text{Med}}}{C} = \frac{7.78}{\left(1 + \frac{1}{M}\right)} - 5.67 \geq 1 \tag{29}$$

where $M$ is calculated using Eqs. (8) and (11). Equation (29) is a requirement for the splice length calculation by Eq. (27). Thus, Eq. (27) cannot be used unless the requirement of Eq. (29) is provided.

### 5.1 Comparison between the proposed equation with ACI 440.1R [2] and CAN/CSA S806-02 [7]

The proposed equation is evaluated with respect to the existing design equations (ACI 440.1R-06 guidelines [3] and CAN/CSA S806-02 code [5]) using the experimental results and also by performing a parametric study. As mentioned earlier, the ACI 440.1R-06 guidelines [3] and CAN/CSA S806-02 code [5] overestimate the bond strength between concrete and GFRP bars for the current test series. Therefore, the probability of bond failure of GFRP bars increases in lap-spliced beams designed with these provisions. This fact can also be concluded from Figs. 4 and 5. Figures 4 and 5 show plots of the experimentally

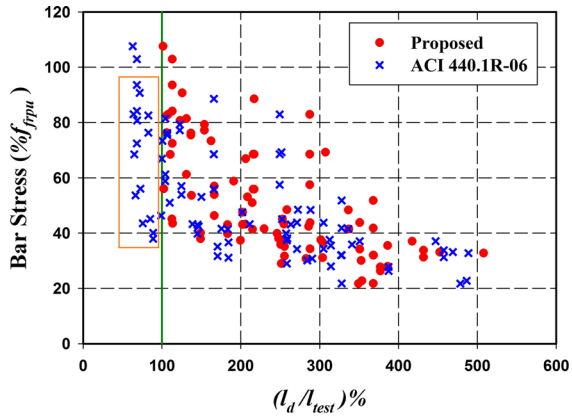


**Fig. 4** Comparison between the proposed equation and ACI 440.1R-06 guidelines [3] with the test results

achieved bar stress as a percentage of the ultimate tensile strength versus the predicted splice length using the three design equations as a percentage of the test splice length. It should be noted that the predicted design lengths by ACI 440.1R-06 guidelines [3] (Fig. 4) and CAN/CSA S806-02 code [5] (Fig. 5) include the factors 1.3 and 1.6, respectively. In each of these figures, the x-axis is the splice length calculated using the method being displayed divided by the test splice length. It is expected that the mode of failure should be bar fracture (or at least achievement of 100% $f_{fu}$) for the bars have splice length longer than the calculated splice length, whereas the bars have splice length a distance shorter than the calculated splice length would be provided to experience a bond failure.

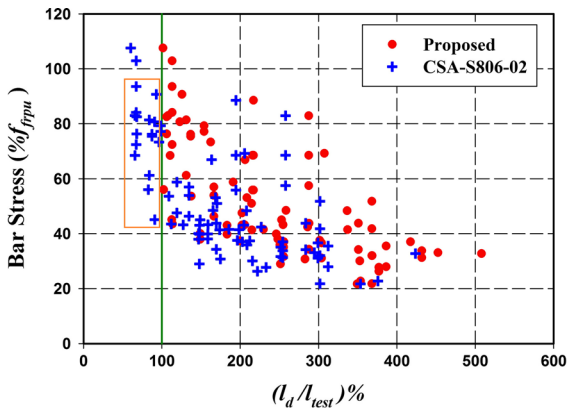


**Fig. 5** Comparison between the proposed equation and CAN/CSA S806-02 code [5] with the test results

As seen in Figs. 4 and 5, some experimental specimens shown by solid rectangle had splice lengths greater than the splice lengths determined by ACI 440.1R-06 guidelines [3] and CAN/CSA S806-02 code [5]. However, they failed with bar stresses lower than the ultimate tensile strengths. This shows that ACI 440.1R-06 guidelines [3] and CAN/CSA S806-02 code [5] usually underestimate the splice length. As shown in Figs. 4 and 5, these specimens (shown by solid rectangle (have lengths smaller than the splice lengths specified by the proposed equation. To show the conditions under which the proposed equation predicts a longer splice length compared to ACI 440.1R-06 guidelines [3] and CAN/CSA S806-02 code [5], a parametric study is performed. The results of the study are illustrated in Fig. 6, which shows the predicted splice length versus $C/d_b$ relationship for

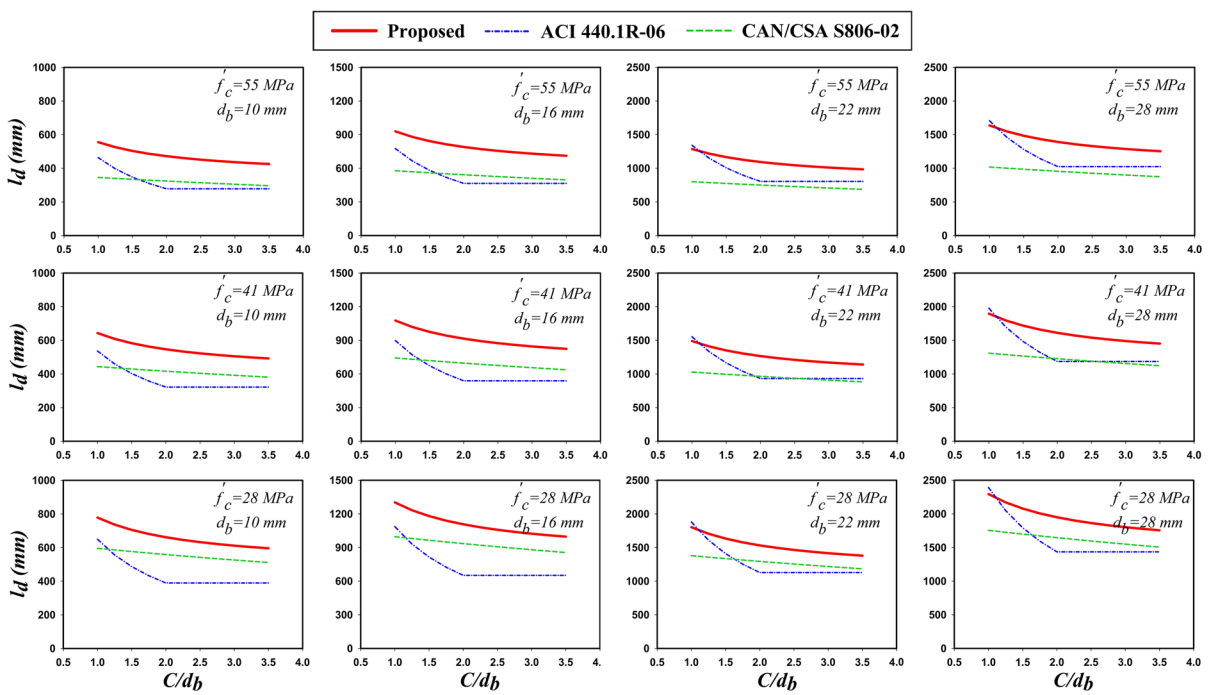


**Fig. 6** Comparison between the proposed equation with ACI 440.1R-06 guidelines [3] and CAN/CSA S806-02 code [5]

different bar sizes and concrete strengths. For each bar size, the clear cover varied between $1d_b$ and $3.5d_b$ values. According to Fig. 6, the splice length obtained from the proposed equation is larger than those predicted by the ACI 440.1R-06 guidelines [3] and CAN/CSA S806-02 code [5] provisions. Thus, these provisions underestimate the splice length of GFRP bars.

## 6 Conclusions

The objective of this study was to utilize available experimental data to propose equations for the bond strength and splice length of GFRP bars in beams with spliced bars. All of the parameters which influence the bond strength were taken into account in the proposed equation. Based on the study, the following conclusions can be drawn:

1. Using the eccentric pullout test results, an equation was obtained for local bond strength between GFRP bars and concrete. The local bond strength calculated by this equation has good agreement with the experimental results.
2. In the proposed equation for bond strength of spliced GFRP bars, the non-uniform distribution of bond stress and the modulus of elasticity of GFRP bars were taken into account. When compared to other equations, the proposed equation predicted the bond strength of tensile splices most accurately. It was shown that, the ACI 440.1R-06 guidelines [3], CAN/CSA S806-02 [5] and CAN/CSA S6-06 [6] codes overestimate the bond strength of GFRP bars in concrete beams with lap-spliced bars for the current test series.
3. A simple and practical equation was proposed for determining the splice length in concrete beams with spliced GFRP bars. When compared to the ACI 440.1R-06 guidelines [3] and CAN/CSA S806-02 code [5], the proposed equation generally requires a larger splice length.

### Compliance with ethical standards

**Conflict of interest** The authors declare that they have no conflict of interest.

## References


1. Golafshani EM, Rahai A, Sebt MH (2014) Bond behavior of steel and GFRP bars in self-compacting concrete. Constr Build Mater 61(30):230–240
2. Mosley CP, Tureyen AK, Frosch RJ (2008) Bond strength of nonmetallic reinforcing bars. ACI Struct J 105(5):634–642
3. ACI Committee 440.1R-06 (2006) Guide for the design and construction of structural concrete reinforced with FRP bars. American Concrete Institute, Michigan
4. Lin X, Zhang YX (2014) Evaluation of bond stress-slip models for FRP reinforcing bars in concrete. Compos Struct 107:131–141
5. CAN/CSA S806-02 (2002) Design and construction of building components with fiber reinforced polymers. Canadian Standards Association, Mississauga
6. CAN/CSA S6-06 (2006) Canadian highway bridge design code. Canadian Standards Association, Mississauga
7. Darwin D, Zou J, Tholen M, Idun E (1996) Development length criteria for conventional and high relative rib area reinforcing bars. ACI Struct J 93(3):347–359
8. Orangun CO, Jirsa JO, Breen JE (1977) A reevaluation of test data on development length and splices. Proc ACI J 74(3):114–122
9. Esfandeh M, Sabet AR, Rezadoust AM, Alavi MB (2009) Bond performance of FRP rebars with various surface deformations in reinforced concrete. Polym Compos 30(5):576–582
10. Wambeke B, Shield C (2006) Development length of glass fiber-reinforced polymer bars in concrete. ACI Struct J 103(1):11–17
11. Esfahani MR, Rangan BV (1998) Bond between normal strength and high-strength concrete and reinforcing bars in splices in beams. ACI Struct J 95(3):272–280
12. Aly R (2005) Experimental and analytical studies on bond behavior of tensile lap spliced FRP reinforcing bars in concrete. Dissertation, Department of Civil Engineering, University of Sherbrook, Sherbrook
13. Harajli M, Abouniaj M (2010) Bond performance of GFRP bars in tension: experimental evaluation and assessment of ACI 440 guidelines. ASCE J Compos Constr 14(6):659–668
14. Choi DU, Chun SC, Ha SS (2012) Bond strength of glass fiber-reinforced polymer bars in unconfined concrete. Eng Struct 34:303–313
15. Pay AC, Canbay E, Frosch RJ (2014) Bond strength of spliced fiber-reinforced polymer reinforcement. ACI Struct J 111:257–266
16. Mousavi SR (2011) Evaluation of stiffness and deflection in FRP reinforced concrete beams using modal test and genetic algorithm. Dissertation, Ferdowsi University of Mashhad, Iran
17. Tighiouart B, Benmokrane B, Mukhopadhyaya P (1999) Bond strength of glass FRP rebars splices in beams under static loading. Constr Build Mater 13(7):383–392
18. Esfahani MR, Rakhshanimehr M, Mousavi SR (2013) Bond strength of lap-spliced GFRP bars in concrete beams. ASCE J Compos Constr 17(3):314–323
19. Esfahani MR, Kianoush MR (2005) Development/splice length of reinforcing bars. ACI Struct J 102(1):22–30

20. Tepfers R (1973) A theory of bond applied to overlapped tensile reinforcement splices for deformed bars. In: Chalmers Tekniska Hoegskola Publication 73.2, Division of Concrete Structures, Chalmers University of Technology, Gothenburg, Sweden
21. Esfahani MR, Rangan BV (1998) Local bond strength of reinforcing bars in normal strength and high-strength concrete. ACI Struct J 95(2):96–106
22. Tepfers R, Karlsson M (1997) Pull-out and tensile reinforcement splice tests using FRP C-bars. In: Proceedings of the 3rd international symposium on non-metallic (FRP) reinforcement for concrete structures (FRPRC-3), Sapporo, Japan, pp 357–364
23. Tepfers R, Hedlund G, Rosinski B (1998) Pull-out and tensile reinforcement splice tests with GFRP Bars. In: Saadatmanesh H, Ehsani MR (eds) Fiber composites in infrastructure: proceedings of the 2nd international conference on composites in infrastructure, ICCI 98, Tucson, Arizona, pp 37–51
24. Esfahani MR, Kianoush MR, Lachemi M (2005) Bond strength of glass fiber reinforced polymer reinforcing bars in normal and self consolidating concrete. Can J Civ Eng 32(3):553–560
25. Aly R (2007) Stress along tensile lap-spliced fiber reinforced polymer reinforcing bars in concrete. Can J Civ Eng 34(9):1149–1158
26. Losberg A, Olsson P (1979) Bond failure of deformed reinforcing bars based on the longitudinal splitting effect of the bars. ACI J 76(1):5–18
27. Davalos JF, Chen Y, Ray I (2008) Effect of FRP bar degradation on interface bond with high strength concrete. Cem Concr Compos 30(8):722–730
28. Hao QD, Wang YL, Zhang ZC (2007) Bond strength improvement of GFRP rebars with different rib geometries. J Zhejiang Univ Sci A 8(9):1356–1365
29. Lee J, Kim T, Yi C, Park J, You Y, Park Y (2008) Interfacial bond strength of glass fiber reinforced polymer bars in high-strength concrete. Compos Part B Eng 39(2):258–270
30. Banea M, Torres L, Turon A, Barris A (2009) Experimental study of bond behavior between concrete and FRP bars using a pull-out test. Compos Part B Eng 40(8):784–797
31. Okelo R, Yuan R (2005) Bond strength of fiber reinforced polymer rebars in normal strength concrete. ASCE J Compos Constr 9(3):203–213
32. Pillai SU, Krik DW (1988) Reinforced concrete design, 2nd edn. McGraw-Hill Ryerson, Toronto
33. Rezansoff T, Akanni A, Sparling B (1993) Tensile lap splices under static loading: a review of the proposed ACI 318 code provisions. ACI Struct J 90(4):374–384
34. Quayyum S (2010) Bond behaviour of fiber reinforced polymer (FRP) rebars in concrete. Dissertation, Department of Civil Engineering, University of British Columbia, Kelowna, Canada